Helical Structure of the COOH Terminus of S3 and Its Contribution to the Gating Modifier Toxin Receptor in Voltage-gated Ion Channels

Yingying Li-Smerin and Kenton J. Swartz

From the Molecular Physiology and Biophysics Unit, National Institute of Neurological Disorders and Stroke, National Institutes of Health, Bethesda, Maryland 20892

ABSTRACT The voltage-sensing domains in voltage-gated K^+ channels each contain four transmembrane (TM) segments, termed S1 to S4. Previous scanning mutagenesis studies suggest that S1 and S2 are amphipathic membrane spanning α-helices that interface directly with the lipid membrane. In contrast, the secondary structure of and/or the environments surrounding S3 and S4 are more complex. For S3, although the NH_2-terminal part displays significant helical character in both tryptophan- and alanine-scanning mutagenesis studies, the structure of the COOH-terminal portion of this TM is less clear. The COOH terminus of S3 is particularly interesting because this is where gating modifier toxins like Hanatoxin interact with different voltage-gated ion channels. To further examine the secondary structure of the COOH terminus of S3, we lysine-scanned this region in the *drk1* K^+ channel and examined the mutation-induced changes in channel gating and Hanatoxin binding affinity, looking for periodicity characteristic of an α-helix. Both the mutation-induced perturbation in the toxin–channel interaction and in gating support the presence of an α-helix of at least 10 residues in length in the COOH terminus of S3. Together with previous scanning mutagenesis studies, these results suggest that, in voltage-gated K^+ channels, the entire S3 segment is helical, but that it can be divided into two parts. The NH_2-terminal part of S3 interfaces with both lipid and protein, whereas the COOH-terminal part interfaces with water (where Hanatoxin binds) and possibly protein. A conserved proline residue is located near the boundary between the two parts of S3, arguing for the presence of a kink in this region. Several lines of evidence suggest that these structural features of S3 probably exist in all voltage-gated ion channels.

KEY WORDS: secondary structure • scanning mutagenesis • voltage-dependent gating • Fourier transformation

INTRODUCTION

Voltage-gated K^+ channels are tetrameric membrane proteins that contain six transmembrane (TM)[1] segments per subunit (see Fig. 1 A). The first four TMs are thought to form the voltage-sensing domains, whereas the fifth through sixth TMs assemble to form the pore domain (Kubo et al., 1993; Doyle et al., 1998; Li-Smerin and Swartz, 1998; Yellen, 1998; Li-Smerin et al., 2000). Our understanding of the pore domain structure has been guided by the crystal structure of the bacterial KcsA K^+ channel (Doyle et al., 1998; MacKinnon et al., 1998), a relatively simple K^+ channel (Schrempf et al., 1995) that lacks the voltage-sensing domains found in voltage-gated K^+ channels. Although the 3-D structure of the voltage-sensing domains has not yet been obtained, scanning mutagenesis studies have provided information about the likely secondary structure of the TMs contained therein (Monks et al., 1999; Hong and Miller, 2000; Li-Smerin et al., 2000). These scanning approaches rely on a bimodal environment surrounding the presumed helix to detect underlying periodicity in secondary structure. The premise is that mutations will be tolerated at interfaces with solvent (either lipid or water) as long as the substituted side chain is solvent compatible, but that they will be poorly tolerated at protein-protein interfaces. Both tryptophan-scanning mutagenesis in the *Shaker* K^+ channel (Monks et al., 1999; Hong and Miller, 2000) and alanine-scanning mutagenesis in the *drk1* K^+ channel (Li-Smerin et al., 2000) suggest that at least portions of S1 through S4 adopt an α-helical secondary structure. The scans of S1 and S2 suggest that these segments are relatively simple amphipathic α-helices that span the full width of the membrane and make extensive contacts with the lipid membrane. In contrast, only portions of S3 and S4 display helical character. For example, the alanine-scan of S4 detected helical periodicity in only the COOH-terminal region (Li-Smerin et al., 2000). Since the entire S4 segment consists of a repeating triplet of a basic and two hydrophobic residues, it seems likely that the secondary structure of the full-length of S4 is helical and that the absence of helical character in the NH_2-termi-

Address correspondence to Kenton J. Swartz, Molecular Physiology and Biophysics Unit, National Institute of Neurological Disorders and Stroke, National Institutes of Health, Building 36, Room 2C19, 36 Convent Drive, MSC 4066, Bethesda, MD 20892. Fax: (301) 435-5666; E-mail: swartzk@ninds.nih.gov

[1]*Abbreviations used in this paper:* α-PI, α-periodicity index; TM, transmembrane.

nal portion results from complexities in the environment surrounding the segment.

The present study focuses on the complexities in the S3 segment. In both tryptophan- and alanine-scanning mutagenesis studies, when the entire S3 segment is considered as a single TM, there is no clear indication of helical structure (Hong and Miller, 2000; Li-Smerin et al., 2000). However, both scanning studies found evidence for helical structure when restricting the analysis to only the NH_2-terminal two thirds of S3, up to a conserved proline residue (Pro268 in drk1). In the alanine scan, which covers the entire region from the NH_2 terminus of S1 through the COOH terminus of S4 (including linkers), an unanticipated peak in the α-periodicity index (α-PI) is observed in the region encompassing the COOH terminus of S3 and the S3–S4 linker. This is illustrated in Fig. 1 B, where a windowed α-periodicity analysis is shown for mutation-induced perturbations in gating for the region spanning from S1 to S4. Although the mutation-induced perturbations in gating were rather weak for the region in question (Li-Smerin et al., 2000), the results hint that the COOH-terminal portion of S3 may have a helical structure.

The COOH-terminal region of S3 is of particular interest because it has been identified as an important region for interaction with various gating modifier toxins (Rogers et al., 1996; Swartz and MacKinnon, 1997b; Li-Smerin and Swartz, 1998, 2000; Winterfield and Swartz, 2000). This is illustrated in Fig. 1 B for Hanatoxin, a 35–amino acid protein isolated from tarantula venom (Swartz and MacKinnon, 1995) that inhibits the *drk1* K^+ channel by shifting activation to more depolarized voltages (Swartz and MacKinnon, 1997a). The alanine scan of the region starting from the NH_2 terminus of S1 to the COOH terminus of S4 in the *drk1* K^+ channel shows that the largest perturbations in toxin binding are located in the COOH terminus of S3 (Swartz and MacKinnon, 1997b; Li-Smerin and Swartz, 2000). In principle, the distribution of residues whose mutation alters toxin binding should also contain information about the secondary structure of the COOH terminus of S3. Although, the three positions where mutations had large effects on toxin binding (I273, F274, and E277) are distributed in a manner consistent with helical structure, clearly additional positions with large perturbations are needed to further examine this hint of secondary structure. The dimensions of Hanatoxin (~20 × 25 Å) strongly suggest that many channel residues are located at the interface between toxin and channel (Takahashi et al., 2000). Perhaps, mutations more disruptive than substitutions to alanine may help to identify additional channel residues at the toxin–channel interface.

In this study, we systematically mutated 20 residues (one at a time) in the COOH terminus of S3 and the S3–S4 linker in the *drk1* K^+ channel to Lys to further evaluate the secondary structure of this region and to explic-

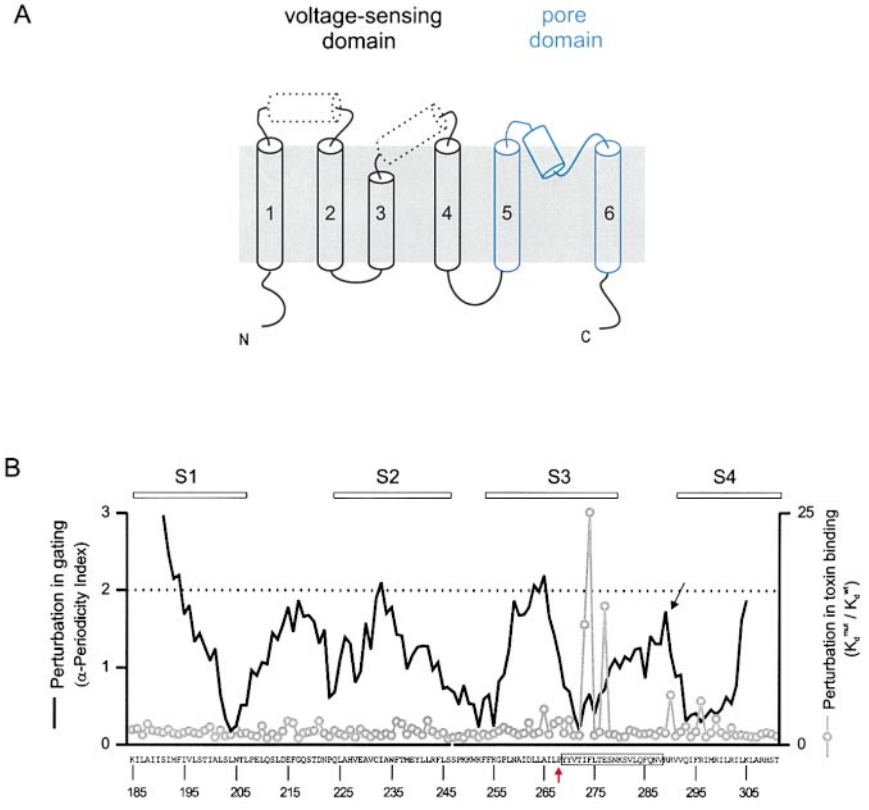

FIGURE 1. (A) Putative topology of a single subunit of a tetrameric voltage-gated K^+ channel with six transmembrane helices. The top is extracellular and the bottom is intracellular (Li-Smerin et al., 2000). (B) Results of previous alanine-scanning mutagenesis in the region of S1 to S4 in the *drk1* K^+ channel (Li-Smerin et al., 2000). Solid line is a windowed α-PI analysis (13-residue window) for perturbations in gating. Dotted line marks the value of 2 for α-PI. Open circles connected with straight lines are perturbations in Hanatoxin binding affinity (K_d^{mut}/K_d^{wt}) caused by Ala substitutions (Li-Smerin and Swartz, 2000). Horizontal open bars above the plot demarcate the approximate positions of the four transmembrane segments as indicated by the Kyte-Doolittle hydrophobicity analysis (Kyte and Doolittle, 1982). Letters and numbers indicate the wild-type residues and their positions. Red arrow highlights the Pro residue conserved in the voltage-gated K^+ channels (see Fig. 8). The box indicates the stretch of residues mutated to Lys in this study.

itly test the idea that an aqueous environment surrounds at least a portion of this region. The notion of water-exposed surfaces within S3 is based on the fact that Hanatoxin is a water-soluble toxin that presumably interacts with regions of the channel exposed to the extracellular aqueous environment. This is in contrast to S1, S2, and the NH_2 terminus of S3, where the primary surrounding solvent appears to be lipid. We looked for helical periodicity in both the mutation-induced perturbation in Hanatoxin binding and in channel gating. As anticipated, the lysine scan resulted in larger perturbations at a greater number of positions, as compared with the previous alanine scan. Our results argue for α-helical secondary structure of the COOH terminus of S3, and suggest that one face of this helix is exposed to an aqueous environment where the toxin interfaces with the channel.

MATERIALS AND METHODS

Mutagenesis and Channel Expression

Point mutations in *drk1* K^+ channels were introduced by generating mutant fragments by PCR and ligating into appropriately digested vectors. The construct used contained several previously introduced unique restriction sites (Swartz and MacKinnon, 1997b). Mutations were confirmed by automated DNA sequencing. cDNAs encoding wild-type and mutant channels were linearized with NotI and transcribed with T7 RNA polymerase. Oocytes from *Xenopus laevis* frogs were removed surgically and incubated with agitation for 1–1.5 h in a solution containing (in mM): 82.5 NaCl, 2.5 KCl, 1 $MgCl_2$, 5 HEPES, and 2 mg/ml collagenase (Worthington Biochemical Corp.), pH 7.6 with NaOH. Defolliculated *Xenopus* oocytes were injected with cRNA and incubated at 17°C in a solution containing (in mM): 96 NaCl, 2 KCl, 1 $MgCl_2$, 1.8 $CaCl_2$, 5 HEPES, and 50 μg/ml gentamicin (GIBCO BRL), pH 7.6 with NaOH for 1–4 d before recording.

Electrophysiology

Two-electrode voltage-clamp recordings were performed to study the toxin–channel interaction or the voltage-dependent gating behavior using an oocyte clamp (model OC-725C; Warner Instruments). Oocytes were perfused in a 160-μl recording chamber with a solution containing (in mM): 50 RbCl, 50 NaCl, 1 $MgCl_2$, 0.3 $CaCl_2$, and 5 HEPES, pH 7.6. Data were filtered at 2 kHz (eight-pole Bessel) and digitized at 10 kHz. Microelectrodes were filled with 3 M KCl and had resistances between 0.2 and 1.0 MΩ. All experiments were conducted at room temperature (~22°C).

The voltage was typically held at −110 to −80 mV where no steady-state inactivation could be detected. For most channels, inward tail current (carried by Rb^+ to slow the deactivation) was elicited by repolarization to −50 mV, and the amplitude of the tail current was measured 2–3 ms after repolarization. For the mutant channels that had large leftward shifts in the voltage-activation relationship, more negative tail voltages were used. For some mutant channels with large rightward shifts in the voltage-activation relationship, 0 to +20 mV was used to elicit an outward tail current.

Analysis of Toxin–Channel Interaction

The concentration dependence for occupancy of the channel by Hanatoxin was examined as previously described (Swartz and MacKinnon, 1997a; Li-Smerin and Swartz, 2000). We used at least two concentrations of Hanatoxin (between 100 and 250 μM) to initially evaluate the binding affinity of Hanatoxin to each mutant channel. The equilibrium dissociation constant (K_d) for Hanatoxin was calculated according to:

$$K_d = \left(\frac{1}{1-(I^n/I_0^n)^{1/4}} - 1\right)[\text{toxin}].$$

This equation assumes that there are four independent and equivalent binding sites on the *drk1* K^+ channel for Hanatoxin (Swartz and MacKinnon, 1997a). For the mutant channels that show altered gating properties, we adjusted all voltage protocols appropriately to ensure that the plateau phase in the I/I_0-voltage relation was clearly defined. For mutant channels showing >10-fold change in toxin K_d in the initial screen, three to six toxin concentrations were tested, and the concentration dependence for toxin occupancy was examined as shown in Fig. 3 A. In these instances, the K_d for toxin binding was obtained by fitting a form of the above equation to the data. The change in the free energy of toxin binding ($\Delta\Delta G_T$) was calculated for each mutant channel based on $\Delta\Delta G_T = -RT\ln(K_d^{mut}/K_d^{wt})$.

Analysis of Channel Gating

To evaluate mutation-induced perturbations in channel gating, we regarded the channel as having two states, closed and open, with a single transition between them. Voltage-activation relations were fit with single Boltzmann functions (see Fig. 5) according to:

$$I/I_{max} = (1 + e^{-zF(V-V_{50})/RT})^{-1},$$

where I/I_{max} is the normalized tail current amplitude, z is the equivalent charge, V_{50} is the half-activation voltage, F is Faraday's constant, R is the gas constant, and T is temperature in Kelvin. The difference in Gibbs free energy between closed and open states at 0 mV (ΔG_0) was calculated according to $\Delta G_0 = 0.2389\, zFV_{50}$. The change in ΔG_0 caused by each mutation $\Delta\Delta G_0$) was calculated as $\Delta\Delta G_0 = \Delta G_0^{mut} - \Delta G_0^{wt}$.

Analysis of Periodicity

Fourier transform methods (Cornette et al., 1987; Komiya et al., 1988; Rees et al., 1989a,b) were used to evaluate the periodicity of either $\Delta\Delta G_T$ (toxin binding) or $\Delta\Delta G_0$ (channel gating) for mutations according to the following equation:

$$P(\omega) = (X(\omega)^2 + Y(\omega)^2),$$

$$X(\omega) = \sum_{j=1}^{n}((V_j - \langle V\rangle)\sin(j\omega))$$

and

$$Y(\omega) = \sum_{j=1}^{n}((V_j - \langle V\rangle)\cos(j\omega)),$$

where $P(\omega)$ is the Fourier transform power spectrum as a function of angular frequency ω, n is the number of residues within a segment, V_j is $\Delta\Delta G_T$ or $|\Delta\Delta G_0|$ at a given position j, and <V> is the average value of $\Delta\Delta G_T$ or $|\Delta\Delta G_0|$ for the segment.

The α-PI (Cornette et al., 1987; Komiya et al., 1988) was calculated to quantitatively evaluate the α-helical character from the power spectra according to the following equation:

$$\alpha\text{-PI} = \left[1/30 \int_{90°}^{120°} P(\omega)d\omega\right] \Big/ \left[1/180 \int_{0°}^{180°} P(\omega)d\omega\right].$$

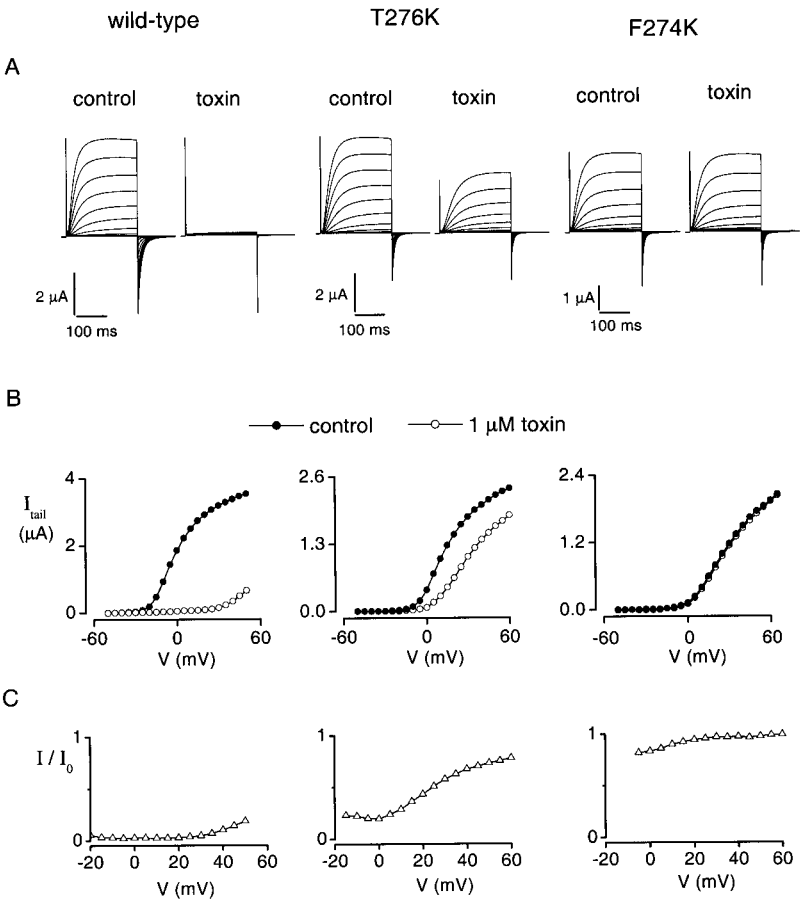

FIGURE 2. Hanatoxin inhibition of the *drk1* K^+ channel. (A) Families of current records obtained with two-electrode voltage-clamp techniques from oocytes expressing wild-type (left), and two mutant *drk1* K^+ channels (middle, T276K; and right, F274K). The holding voltage was −80 mV. Currents were elicited by depolarizing steps starting at −50 mV and incrementing in 5-mV steps in the absence (left) and presence of 1 μM toxin (right). Tail currents were elicited by repolarization to −50 mV. 15 traces are shown for the wild-type (−50 to +20 mV), and 17 traces are shown for either T276K or F274K (−50 to +30 mV). All traces are shown without subtraction of the leak or capacitive currents. (B) Voltage-activation relations for wild-type (left), T276K (middle), and F274K (right). Tail current amplitude was measured 2–3 ms after repolarization in the absence and presence of 1 μM toxin as indicated. Data are from the same oocytes presented in A. (C) Fraction of uninhibited tail current calculated from the corresponding data presented in B. I is the tail current measured in the presence of 1 μM toxin, and I_0 is the tail current measured in the absence of toxin.

RESULTS

As defined by hydrophobicity analysis, the S3 segment in the *drk1* K^+ channel begins around F254 and ends near S278. The region we focused on in this study begins immediately after P268 in S3 and ends at V288, near the NH_2 terminus of S4 (Fig. 1 B). Our hypothesis was that at least part of this region adopts an α-helical secondary structure, with one face of the helix interacting with water and constituting a major part of the receptor for gating modifier toxins. In contrast, a distinct face of the helix may interact in some way with other elements of the voltage-sensing domain. To test this hypothesis, we mutated each residue to Lys and examined both the effects on Hanatoxin binding affinity and on the gating behavior of the channel. We chose to mutate to Lys, a large and basic amino acid, with the hope that it would produce more robust perturbations in protein–protein interactions compared with the previous alanine scan. In addition, the hydrophilic nature of the Lys sidechain should discriminate between protein–protein and protein–solvent interfaces where the solvent is water. We anticipated that residues whose mutation altered toxin binding would show helical distributions and be well tolerated with respect to perturbations in gating because, in the absence of the toxin, they interact with water. The positions where mutations do not influence toxin binding might be predicted to strongly influence gating if they interact with other elements within the channel protein.

Perturbation of the Toxin–Channel Interaction with Lysine Substitutions

First, we tested whether Lys substitutions at each of the 20 residues perturb Hanatoxin binding to the channel. Wild-type and mutant channels were expressed in *Xenopus* oocytes and the inhibition by Hanatoxin was examined using two-electrode voltage-clamp recording techniques. We measured the fractional inhibition of tail currents carried by 50 mM Rb^+ at various toxin concentrations. Fig. 2 shows the inhibitory effect of 1 μM Hanatoxin on the wild-type (left) and two exemplary mutant channels, T276K (middle) and F274K (right). Hanatoxin greatly inhibited the wild-type channel, but only moderately inhibited T276K, and was almost without effect on F274K, as shown by the families of current records (Fig. 2 A) and the tail current voltage-activation relations (Fig. 2 B). To quantitatively evaluate the concentration dependence for toxin occupancy of the channel, we calculated the fraction of uninhibited current for various strength depolarizations (Fig. 2 C).

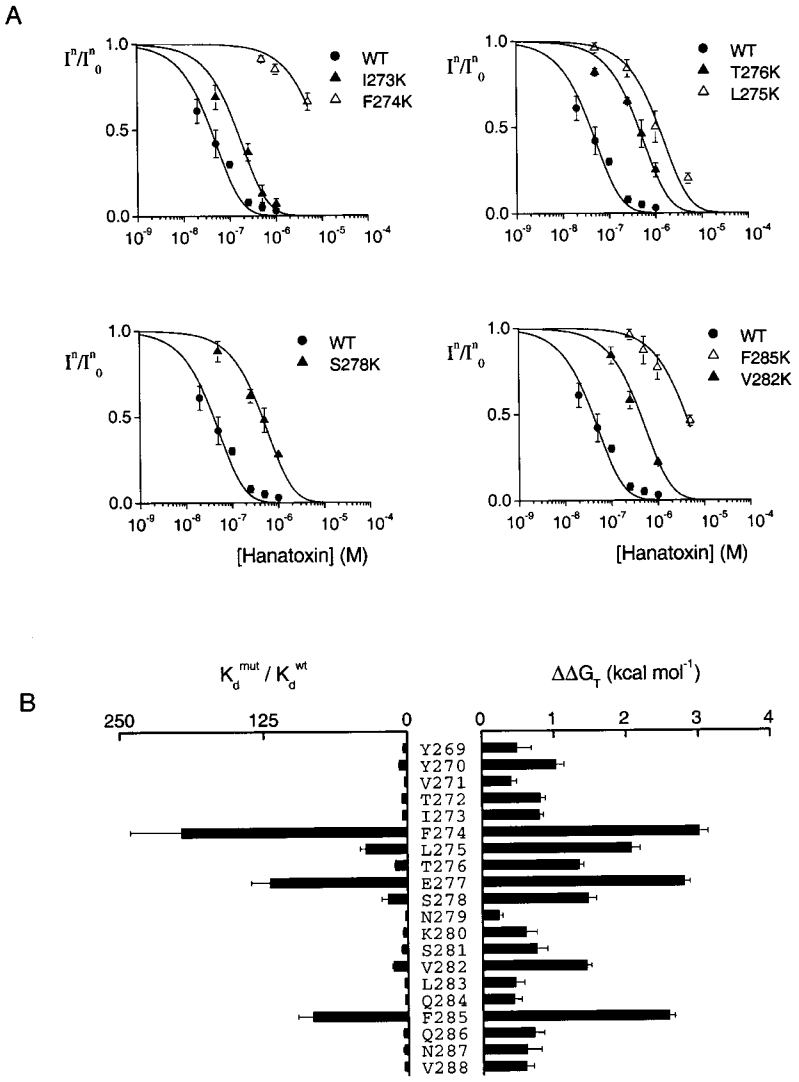

FIGURE 3. Perturbations in toxin binding affinity with Lys substitutions. (A) Concentration dependence for inhibition of the *drk1* K^+ channel by Hanatoxin. I^n/I_0^n is the value of I/I_0 measured in the plateau phase at negative voltages as shown in Fig. 2 C and plotted against toxin concentration for wild-type and seven mutant channels. Symbols are experimental data for the mean ± SEM for 3–12 cells. Solid lines correspond to $I^n/I_0^n = (1 - P)^4$, where $P = [\text{toxin}]/([\text{toxin}] + K_d)$ with the following K_d values (in μM): 0.21 for WT; 0.76 for I273K; 41.5 for F274K; 2.1 for T276K; 6.2 for L275K; 2.4 for S278K; 20.8 for F285K; and 2.0 for V282K. The equation assumes four equivalent binding sites for Hanatoxin on each channel. (B) Perturbations in toxin binding caused by mutations to Lys expressed as fold change (K_d^{mut}/K_d^{wt}) or free energy ($\Delta\Delta G_T$). Data are presented as mean ± SEM for 4–28 cells for each channel. Data for E277K are from (Li-Smerin and Swartz, 2000). All residues were mutated to Lys, except for K280, which was mutated to Asp.

The fraction of uninhibited current (I/I_0) measured in the plateau phase at negative voltages (I^n/I_0^n), where toxin-bound channels do not open, approximates the fraction of unbound channels and, therefore, was used to determine the K_d for toxin binding (see MATERIALS AND METHODS). Fig. 3 A shows the concentration dependence for fractional inhibition of the wild-type and seven mutant channels (I273K, F274K, L275K, T276K, S278K, V282K, and F285K). Fitting of a four site model to the data yielded K_d values of (in μM): 0.21 for the wild type; 0.76 for I273K; 2.1 for T276K; 2.2 for V282K; 2.4 for S278K; 6.2 for L275K; 20.8 for F285K; and 41.5 for F274K. Fig. 3 B summarizes the changes in the K_d values and in the free energy of toxin binding caused by Lys substitutions for all 20 residues. When compared with the previous results with Ala substitutions (Li-Smerin and Swartz, 2000), mutations to Lys identified five additional positions where mutations produce large effects on toxin binding. In addition to the previously described mutations (F274K and E277K), substitution with Lys at L275, T276, S278, V282, and F285 resulted in $\Delta\Delta G_T$ values >1 kcal mol^{-1}. In contrast, Lys substitution at I273 caused a smaller change than did mutation to Ala (0.8 kcal mol^{-1} for Lys vs. 1.6 kcal mol^{-1} for Ala). These results are consistent with previous work identifying the COOH terminus of S3 as a major component of the Hanatoxin receptor and importantly identify additional residues whose mutation influences toxin binding.

Having these newly identified positions in hand, we examined whether the distribution of toxin binding perturbations was consistent with the α-helical structure using Fourier transform methods and both helical wheel and net diagrams. For an ideal amphipathic α-helix, Fourier transform analysis should reveal a predominant peak with an angular frequency of 100° (360°/3.6 residues per turn of the helix). The helical periodicity can be evaluated quantitatively by integrating the power spectrum and calculating the α-PI (see MATERIALS AND METHODS), with values ≥2 indicating

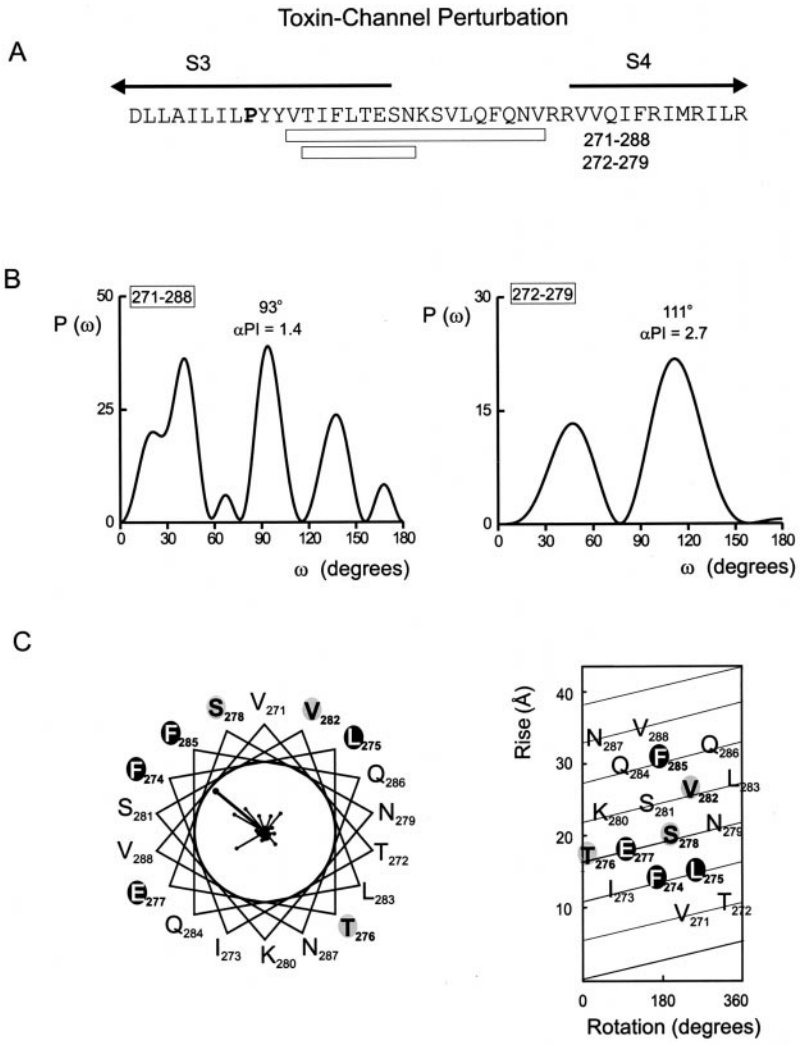

FIGURE 4. Periodicity analysis for perturbations in Hanatoxin binding. (A) Amino acid sequence of a region starting with S3 and ending with S4 of the *drk1* K^+ channel. A conserved Pro residue is highlighted with a bold letter. Arrows above the sequence correspond to portions of S3 and S4 defined by Kyte-Dolittle hydrophobicity analysis. Open bars indicate the stretches of residues used for Fourier transformation analysis. (B) Power spectra of $\Delta\Delta G_T$ values for either 18 (left) or 8 (right) residue stretches, where $P(\omega)$ is plotted as a function of angular frequency (ω). (C) Helical wheel (left) and net (right) diagrams for the 18 residues used for the left power spectrum in B. Black and light gray shaded ovals indicate positions with $\Delta\Delta G_T > 1.5$ kcal mol^{-1} and between 1 and 1.5 kcal mol^{-1}, respectively. Unshaded positions correspond to $\Delta\Delta G_T < 1$ kcal mol^{-1}. Individual $\Delta\Delta G_T$ values are plotted as vectors on the helical wheel (small circles); scale is 0–6 kcal mol^{-1}. The sum of the $\Delta\Delta G_T$ vectors is represented with the large circle and has a magnitude of 5.5 kcal mol^{-1}.

α-helical structure (Rees et al., 1989b). The results of Fourier transform analysis of $\Delta\Delta G_T$ are presented in Fig. 4. The power spectrum of a stretch of 18 residues beginning with V271 and ending with V288 (Fig. 4 B) exhibits a rather complex profile with multiple peaks at different angular frequencies. Although there is a significant peak at 93°, the α-PI value for this spectrum is only 1.4. In contrast, the power spectrum for a shorter stretch (eight residues long), beginning with T272 and ending with N279, reveals a primary peak at 111°, with a rather strong α-PI value of 2.7 (Fig. 4 B, right). When the mutation-induced perturbations are plotted on helical wheel or net diagrams (Fig. 4 C), it is striking that with only one exception the "hot residues" (Fig. 4 C, $\Delta\Delta G_T > 1$ kcal mol^{-1}, black and gray shading) are located on one side of the helical diagram. To quantitatively evaluate the clustering of $\Delta\Delta G_T$ values, we plotted individual $\Delta\Delta G_T$ values as vectors along with the sum vector. The sum vector (5.5 kcal mol^{-1}) is larger than any individual $\Delta\Delta G_T$ value and, therefore, highlights a well-defined face where mutations have the largest effects on toxin binding. These results with perturbations in toxin binding argue that the COOH terminus of S3 adopts an α-helical secondary structure and define a face of the helix that is exposed to an aqueous environment, at least in the conformation of the channel protein to which the toxin binds.

Perturbation of Voltage-Dependent Gating with Lysine Substitutions

We next asked whether the effects of Lys substitutions on channel gating display helical distributions, as previously shown for this region with alanine-scanning mutagenesis (Li-Smerin et al., 2000). Voltage-activation relations were obtained for the wild-type and the 20 Lys mutants described above using two-electrode voltage-clamping recording techniques. The amplitude of tail currents carried by 50 mM Rb^+ was measured for various strength depolarizations and single Boltzmann functions fit to the resulting relations (see MATERIAL AND METHODS). The parameters derived from these fits

were then used to evaluate the difference in free energy between the closed and open states of the channel at 0 mV (ΔG_0) for the wild-type and each mutant channel. The mutation-induced perturbation in gating was calculated as the difference in ΔG_0 between the wild-type and the mutant channels ($\Delta\Delta G_0$).

Fig. 5 A shows families of current records for the wild-type (middle) and two exemplary mutant channels, F285K (left) and F274K (right). Compared with the wild-type channel, activation of F285K was shifted to more negative voltages, whereas activation of F274K was shifted to more positive voltages. Voltage-activation relations for the same channels, along with single Boltzmann fits, are presented in Fig. 5 B. Mutation-induced perturbation energies ($\Delta\Delta G_0$) are shown for all 20 mutants in Fig. 5 C. The smallest perturbations observed were 0.2 kcal mol^{-1} for S281K and N287K, and the largest was 2.4 kcal mol^{-1} for L275K. In general, the perturbations observed for mutations to Lys were significantly larger than those previously observed for mutations to Ala. For the alanine scan there were 6/20 residues with $\Delta\Delta G_0 \geq 1$ kcal mol^{-1} (Li-Smerin et al., 2000), whereas for the lysine-scan, 10/20 residues had $\Delta\Delta G_0 \geq 1$ kcal mol^{-1}. The gating properties derived from Boltzmann fits of the voltage-activation relations along with perturbation energies for all 20 mutant channels are summarized in Table I.

We analyzed the periodicity of gating perturbations with the same approach used above for the toxin–channel interaction. The power spectrum of an 18-residue long stretch (V271-V288) shows a predominant peak at 103° angular frequency and a reasonably strong α-PI value of 1.9 (Fig. 6 B, left). Similar to the results for the toxin–channel interaction, we see multiple peaks in this spectrum of gating perturbations. However, in this case, the peak in the helical frequency is more prominent than the corresponding peak in the toxin–channel interaction perturbations. When the region analyzed was restricted to only 10 residues (overlapping with the short eight-residue stretch used for toxin perturbation analysis), we again obtained a very strong helical profile, as shown in Fig. 6 B (right). We see a primary peak at 106° angular frequency and a very large α-PI value of 3.1. Fig. 6 C shows the distribution of the gating perturbation on a helical wheel (left) or in a net diagram (right). Residues whose mutation resulted in $\Delta\Delta G_0$ values ≥1 kcal mol^{-1} (shaded letters) tend to cluster together, although they occupy a large portion of the wheel compared with the perturbations of the toxin–channel interaction. Individual $|\Delta\Delta G_0|$ values were plotted as vectors in Fig. 6 C. The sum vector had a value (4.6 kcal mol^{-1}) larger than any individual $|\Delta\Delta G_0|$ value. Taken together, the results obtained from perturbations in both the toxin–channel interaction and in gating provide compelling evidence for the presence of an α-helix in the COOH terminus of S3.

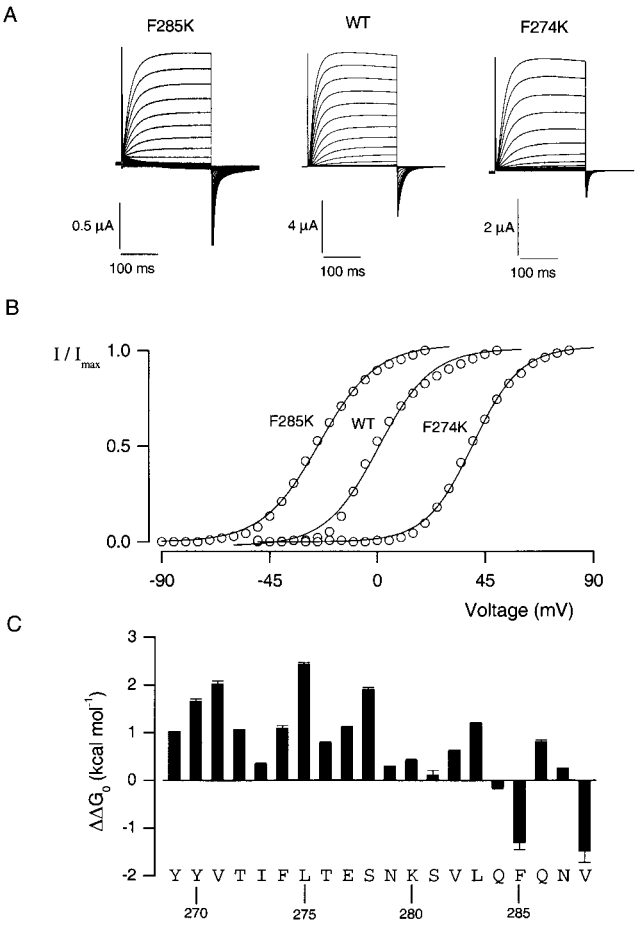

FIGURE 5. Perturbations in gating caused by Lys substitutions. (A) Families of current records obtained with two-electrode voltage-clamp recording for wild-type (middle) and two mutant *drk1* K^+ channels (F285K [left] and F274K [right]). Holding voltage was −90 mV for F285K and −80 mV for WT and F274K. Currents were elicited by voltage steps given in 5-mV increments, and tail currents were elicited by repolarization to −90 mV for F285K and −50 mV for WT or F274K. 23 traces are shown for F285K (−90 to +20 mV) and 19 traces for WT or F274K (−50 to +40 mV). (B) Voltage-activation relations for the three channels in A. Symbols are normalized tail current amplitude measured 2–3 ms after repolarization. Solid lines are single Boltzmann fits to the data. The parameters derived from the fitting are as follows: $V_{50} = -24.3$ mV and $z = 2.2$ for F285K, $V_{50} = +1.2$ mV and $z = 2.4$ for WT, and $V_{50} = +40$ mV and $z = 2.6$ for F274K. (C) $\Delta\Delta G_0$ values calculated (see MATERIALS AND METHODS) for all 20 mutant channels. Data are presented as the mean ± SEM from Table I. Letters and numbers are the native residues and their positions, respectively, within the *drk1* K^+ channel.

DISCUSSION

The goal of this paper was to examine the secondary structure of the COOH terminus of S3 and the S3–S4 linker, a region of voltage-gated ion channels previously shown to be an important component of the receptor

TABLE I

Gating Properties of Wild-type and Mutant drk1 K^+ Channels

	V_{50}	z	ΔG_0	$\Delta\Delta G_0$
	mV		*kcal/mol*	*kcal/mol*
WT	−1.5 ± 0.30	2.7 ± 0.028	-0.095 ± 0.019	
Y269	+25 ± 2.5	1.7 ± 0.12	+0.88 ± 0.022	+0.98 ± 0.022
Y270	+28 ± 0.83	2.3 ± 0.088	+1.5 ± 0.058	+1.6 ± 0.058
V271	+40 ± 1.1	2.0 ± 0.12	+1.8 ± 0.075	+1.9 ± 0.075
T272	+17 ± 0.38	2.4 ± 0.078	+0.9 ± 0.027	+1.0 ± 0.027
I273	+3.9 ± 0.41	2.9 ± 0.067	+0.26 ± 0.028	+0.36 ± 0.028
F274	+24 ± 2.4	2.2 ± 0.82	+1.2 ± 0.17	+1.3 ± 0.17
L275	+43 ± 1.8	2.4 ± 0.11	+2.3 ± 0.056	+2.4 ± 0.056
T276	+15 ± 0.63	2.2 ± 0.072	+0.72 ± 0.028	+0.82 ± 0.028
E277	+15 ± 0.60	2.9 ± 0.081	+1.0 ± 0.025	+1.1 ± 0.025
S278	+24 ± 0.76	3.2 ± 0.16	+1.7 ± 0.045	+1.8 ± 0.045
N279	+2.8 ± 0.36	2.5 ± 0.043	+0.16 ± 0.021	+0.26 ± 0.021
K280	+5.6 ± 0.49	2.5 ± 0.068	+0.31 ± 0.024	+0.41 ± 0.024
S281	+1.4 ± 1.5	2.4 ± 0.085	-0.050 ± 0.091	+0.15 ± 0.091
V282	+9.9 ± 0.64	2.3 ± 0.049	+0.51 ± 0.030	+0.61 ± 0.030
L283	+17 ± 0.010	2.7 ± 0.059	+1.1 ± 0.028	+1.2 ± 0.028
Q284	−4.0 ± 0.64	2.4 ± 0.069	−0.23 ± 0.040	−0.13 ± 0.040
F285	−28 ± 1.4	2.1 ± 0.072	−1.4 ± 0.13	−1.3 ± 0.13
Q286	+12 ± 0.64	2.5 ± 0.079	+0.72 ± 0.050	+ 0.82 ± 0.050
N287	+3.0 ± 0.10	2.1 ± 0.061	+0.14 ± 0.014	+0.24 ± 0.014
V288	−28 ± 1.6	2.2 ± 0.17	−1.5 ± 0.22	−1.4 ± 0.22

The first column indicates the native residues and their positions within the *drk1* K^+ channel. All residues were mutated to Lys except for K280, which was mutated to Asp. V_{50} (the half-activation voltage) and z (the equivalent charge) were derived from fitting single Boltzmann functions to individual voltage-activation relations (see MATERIALS AND METHODS and Fig. 5). ΔG_0 is the free energy difference between closed and open states at 0 mV, and $\Delta\Delta G_0$ is the difference in ΔG_0 between the wild-type and the mutant channel. ΔG_0 and $\Delta\Delta G_0$ were calculated as described in MATERIALS AND METHODS. Data are mean ± SEM for 10–74 voltage-activation relations per channel.

for gating modifier toxins (Rogers et al., 1996; Swartz and MacKinnon, 1997b; Li-Smerin and Swartz, 1998, 2000; Winterfield and Swartz, 2000). We lysine-scanned 20 residues located in this region of the *drk1* K^+ channel and then examined the changes in Hanatoxin binding affinity and channel gating, looking for periodicity characteristic of an α-helix. The strongest indication for helical secondary structure came from analyzing the perturbations in toxin binding and gating for a stretch of 8–10 residues in length that is located within the COOH terminus of S3, as defined by hydrophobicity analysis (Figs. 4 and 6). The analysis of gating perturbations for longer stretches (extended towards S4) was also consistent with a helical structure (Fig. 6), however, the equivalent analysis of perturbations in toxin binding was less clear (Fig. 4). Our results strongly support the existence of an α-helix in the COOH terminus of S3 that is at least ~10 residues long.

What can we say about the environment surrounding this helix? The results from the perturbations in the toxin–channel interaction define a face of a helix in the COOH terminus of S3 that interacts with the toxin. The effects of Hanatoxin on gating currents in the *drk1* K^+ channel suggest that the toxin stabilizes the resting conformation of the voltage-sensing domains (Swartz, 1999). This observation suggests that the toxin-interacting face of the helix in the COOH terminus of S3 is probably exposed to an aqueous environment when the voltage-sensing domains are in a resting conformation that predominates at negative membrane voltages. One of the motivations for substituting with Lys was to explicitly identify water-exposed surfaces within the protein with the assumption that hydrophilic substitutions would be well tolerated at protein–water interfaces. Therefore, we anticipated that the mutations causing little or no perturbation in gating (well tolerated) would cluster together with large perturbations in toxin binding. The helical wheel diagrams in Fig. 7 A show the distributions for the two types of perturbations. Although the distribution in the perturbations in toxin binding and gating are partially distinct, as revealed by ~50° difference between the sum vectors, there is also substantial overlap. One possible explanation for this overlap between the two types of perturbations is that Lys substitutions may perturb gating both by local disruption of protein–protein interactions and

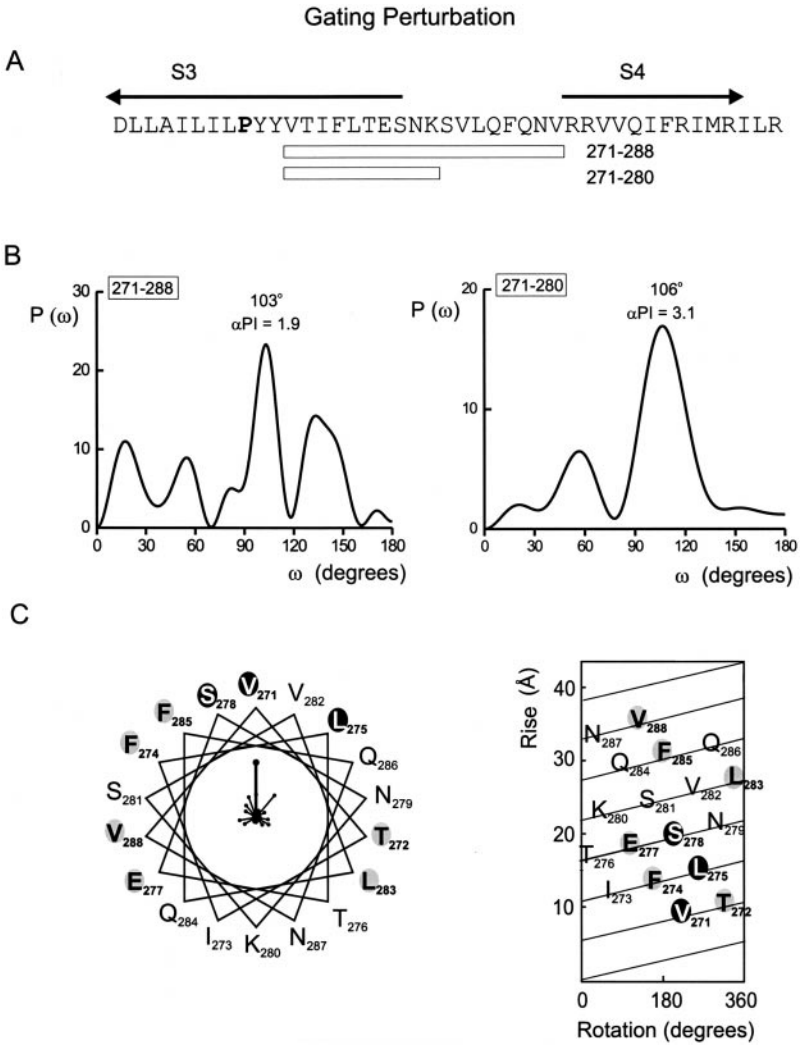

FIGURE 6. Periodicity analysis for perturbations in gating. (A) Amino acid sequence of the region starting with S3 and ending with S4 of the *drk1* K^+ channel (see Fig. 4 legend for details). Open bars indicate the stretches of residues used for Fourier transformation analysis. (B) Power spectra of $|\Delta\Delta G_0|$ values are for either 18 (left) or 10 (right) residues, where $P(\omega)$ is plotted as a function of angular frequency (ω). (C) Helical wheel (left) and net (right) diagrams for the 18 residues used for the left power spectrum in B. Black and light gray shaded ovals indicate positions with $|\Delta\Delta G_0| > 1.5$ kcal mol^{-1} and between 1 and 1.5 kcal mol^{-1}, respectively. Unshaded ovals correspond to $|\Delta\Delta G_0| < 1$ kcal mol^{-1}. Individual $|\Delta\Delta G_0|$ values are plotted as vectors on the helical wheel (small circles); scale is 0–6 kcal mol^{-1}. The sum of the $|\Delta\Delta G_0|$ vectors is represented with the large circle and has a magnitude of 4.6 kcal mol^{-1}.

by more distant electrostatic mechanisms. However, the contribution of electrostatic effects cannot entirely explain the discrepancy because the alanine scan shows very similar shifts in the direction of the sum vectors (~60°) for the perturbations in toxin binding and gating (Fig. 7 B). An alternate explanation is that the region in question undergoes a structural rearrangement during activation, and that this movement causes a change in the solvent exposure of some residues. The voltage-dependent changes in conformation and/or environments surrounding fluorophores introduced at positions near S4 have been previously studied rather extensively (Mannuzzu et al., 1996; Cha and Bezanilla, 1997, 1998; Cha et al., 1998,1999; Gandhi et al., 2000). However, the position closest to the COOH terminus of S3 where fluorophores have been introduced is S346 in the *Shaker* K^+ channel. Based on our sequence alignments, this position is in a region of the S3–S4 linker that is not present in the *drk1* K^+ channel (see last paragraph of DISCUSSION and Fig. 8). Thus, as far as we are aware, no studies have addressed whether the COOH terminus of S3 moves during activation.

Perhaps one of the most interesting aspects of the COOH terminus of S3 is that it forms a canonical binding site for gating modifier toxins in all types of voltage-gated cation channels (Rogers et al., 1996; Swartz and MacKinnon, 1997b; Li-Smerin and Swartz, 1998, 2000; Winterfield and Swartz, 2000). Can we extrapolate from the present work in K^+ channels to voltage-gated Ca^{2+} and Na^+ channels? Examination of the S3 sequences from different voltage-gated channels provides some insight (Fig. 8). First, the residues in the NH_2 terminus of S3 that are most conserved among K^+ channels are also well conserved in the Ca^{2+} and Na^+ channels (Fig. 8, bold letters). Second, although the sequence of the COOH terminus of S3 is less conserved between voltage-gated channels, it is a common target for gating modifier toxins, some of which have been shown to cross-react between the three voltage-gated ion channel types (Chuang et al., 1998; Li-Smerin and Swartz, 1998).

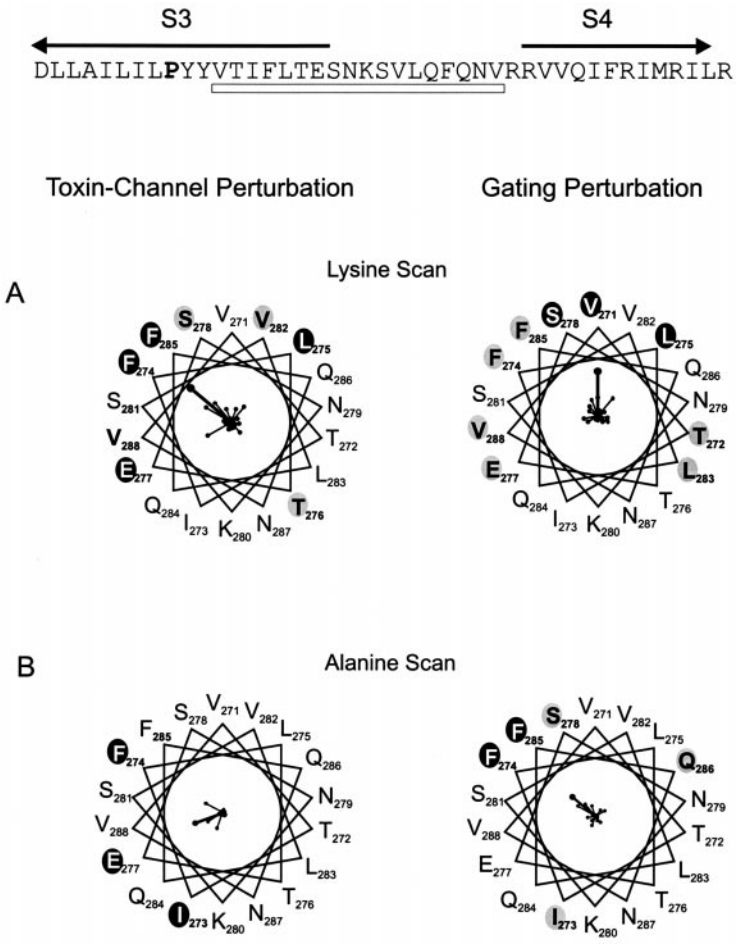

FIGURE 7. Comparison between lysine and alanine scans for perturbations in toxin binding and gating. (A) Helical wheel diagrams for perturbations in toxin binding ($\Delta\Delta G_T$) (left) and gating ($|\Delta\Delta G_0|$) (right) with Lys substitutions. Same plots as in Fig. 4 C and Fig. 6 C. Black and light gray ovals indicate positions with perturbation energies > 1.5 kcal mol^{-1} and between 1 and 1.5 kcal mol^{-1}, respectively. Unshaded positions correspond to perturbation energies <1 kcal mol^{-1}. (B) Helical wheel diagrams for perturbations in toxin binding ($\Delta\Delta G_T$) (left) and gating ($|\Delta\Delta G_0|$) (right) with Ala substitutions. Data are from previously published articles (Li-Smerin and Swartz, 2000; Li-Smerin et al., 2000). Shading has the same meaning as in A. The sum vector for $\Delta\Delta G_T$ has a magnitude of 2.9 kcal mol^{-1}, whereas that for $|\Delta\Delta G_0|$ has a magnitude of 3.1 kcal mol^{-1}. The scale for all vector plots (A and B) is 0–6 kcal mol^{-1}, except that for $\Delta\Delta G_T$ in the alanine scan which is -0.1 to 5.9 kcal mol^{-1}.

Third, Glu residues (Fig. 8, highlighted in red) that are critical determinants of gating modifier toxin receptors in voltage-gated Ca^{2+} channels (Winterfield and Swartz, 2000), Na^+ channels (Rogers et al., 1996) and K^+ channels are located at equivalent positions in S3 (Fig. 8). All of these points suggest that the 3-D structure of this region has been conserved between voltage-gated K^+, Ca^{2+}, and Na^+ channels. Thus, it seems likely that the COOH terminus of S3 is helical and has significant water exposure in all voltage-gated channels.

Previous scanning mutagenesis results uncovered evidence for a helical structure in the NH_2-terminal two thirds of S3 and suggest that, unlike the COOH-terminal part, it is surrounded by lipid and protein (Hong and Miller, 2000; Li-Smerin et al., 2000). Thus, while most of S3 seems to adopt an α-helical structure, the environments surrounding the NH_2- and COOH-terminal portions are quite different. It is interesting that there is a conserved Pro residue located near the junction between the two parts of S3 in voltage-gated K^+ channels (Figs. 1 B and 8). The helix destabilizing effects of Pro residues are well established (O'Neil and DeGrado, 1990; MacArthur and Thornton, 1991; Blaber et al., 1993; Monne et al., 1999). Thus, we speculate that S3 is composed of two α-helices (termed $S3_N$ and $S3_C$ in Fig. 8) separated by a short nonhelical stretch or kink near the conserved Pro residue. It is noteworthy that the Pro residue that is conserved in K^+ channels is conspicuously absent in the voltage-gated Ca^{2+} or Na^+ channels. Instead, these channels most commonly have Gly or Ser residues at positions that are equivalent or adjacent to that of the Pro in K^+ channels (Fig. 8, boxed positions). Like Pro, the helix destabilizing effects of Gly are well known (O'Neil and DeGrado, 1990; MacArthur and Thornton, 1991; Blaber et al., 1993; Monne et al., 1999). Although the helical propensity of the Ser residue in soluble proteins is not particularly low (Blaber et al., 1993), in membrane proteins Ser has a tendency to hydrogen bond with backbone carbonyls, thereby destabilizing the helix (Gray and Matthews, 1984). We examined the crystal structures of six integral membrane proteins and tabulated the residues typically found at kinks in TM helices (Table II). Gly was the most common residue found (33%) at the 36 kinks examined, followed by Pro and Ser, each of which was observed at a frequency of 22%. These observations fit nicely with the idea that there is a kink that separates the two helical parts of S3 not only in

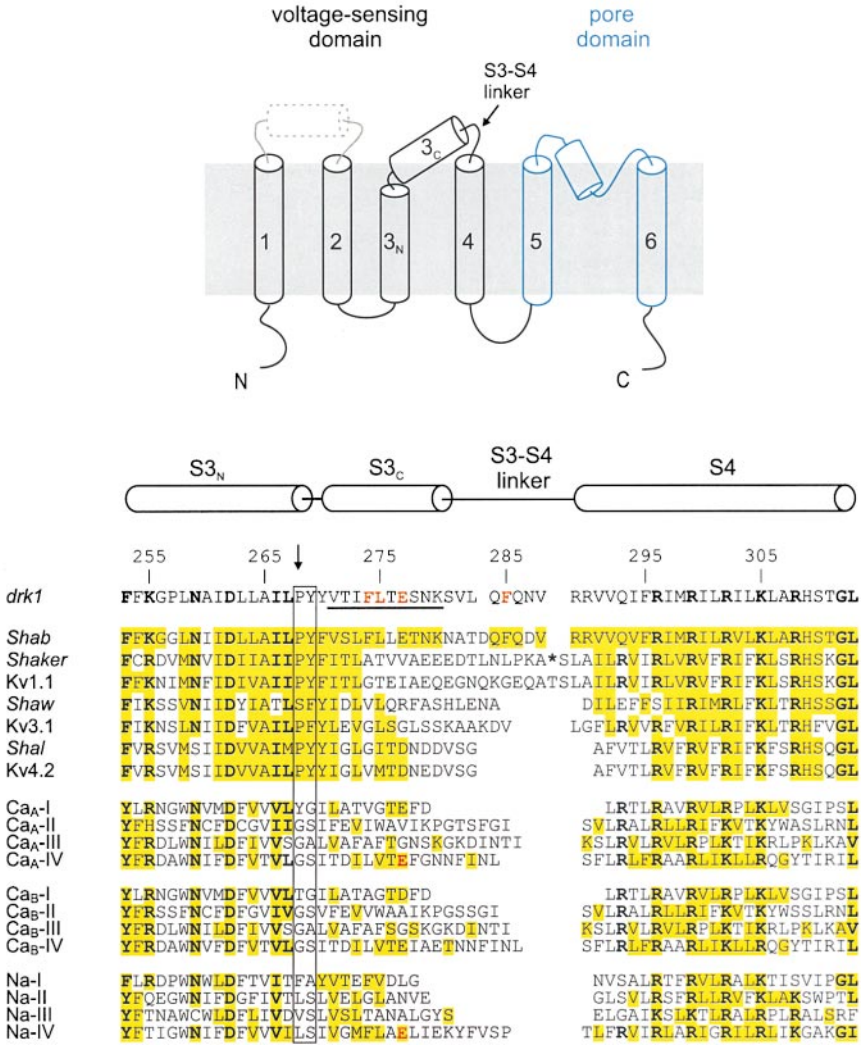

FIGURE 8. α-Helical secondary structure of the gating modifier toxin-binding region in voltage-gated ion channels. The top panel shows the topology of single subunit of the voltage-gated K^+ channel with six transmembrane helices (solid cylinders). The S3 transmembrane segment is shown as having two parts ($S3_N$ and $S3_C$) with a possible kink between them. The bottom panel shows the sequence alignment for the region starting with the NH_2 terminus of S3 and ending with the COOH terminus of S4 for voltage-gated K^+, Ca^{2+}, and Na^+ channels. Horizontal cylinders indicate the approximate positions of S3 (divided into $S3_N$ and $S3_C$) and S4 segments. Numbers indicate the residue positions within the *drk1* K^+ channel, with an arrow marking a Pro residue that is conserved in K^+ channels. The underline highlights the stretch of residues where a strong α-helical character was observed in the present study (Figs. 4 and 6). The yellow highlighting indicates similarity to *drk1*, and bold letters indicate residues that are highly conserved among the three types of the voltage-gated ion channels. For the *Shaker* K^+ channel, 13 residues have been left out (for alignment purposes) and their position is marked by the asterisk. Red letters indicate residues whose mutations cause large changes in the binding affinity of gating modifier toxins (see DISCUSSION).

voltage-gated K^+ channels, but also in voltage-gated Na^+ and Ca^{2+} channels.

Several studies point to the existence of a water-filled vestibule surrounding the S4 helix (Larsson et al., 1996; Mannuzzu et al., 1996; Yang et al., 1996; Cha and Bezanilla, 1997, 1998; Sorensen et al., 2000). In the *Shaker* K^+ channel, the S3–S4 linker has been proposed to contribute to forming this aqueous vestibule (Sorensen et al., 2000). Our results in the *drk1* K^+ channel suggest that the helix in $S3_C$ extends from around V271 to near K280 (Fig. 8, underlined sequence). This leaves only a relatively short S3–S4 linker in this K^+ channel before the presumed beginning of the S4 segment. It is interesting that, according to our designations, the S3–S4 linker is virtually absent in some K^+ channels (e.g., Kv4 family) and several repeats of both voltage-gated Ca^{2+} and Na^+ channels. In contrast, the *Shaker* K^+ channel stands out among the voltage-gated ion channels as having an unusually long S3–S4 linker. Importantly, the region within the S3–S4 linker of the *Shaker* K^+ channel where both thiosulfonates and fluorescence probes have been introduced is not present in most voltage-gated ion channels. Thus, whereas the S3–S4 linker may contribute to a vestibule in *Shaker* K^+ channels, it seems unlikely that it makes a fundamental contribution to the aqueous vestibule surrounding the S4 helix in most voltage-gated ion channels. In contrast, $S3_C$ displays significant sequence conservation, is at least partially exposed to water, and is the target of gating modifier toxins. In addition, deletions in the S3–S4 linker of *Shaker* that do not extend into the region corresponding to $S3_C$ generally cause only subtle changes in gating behavior (Mathur et al., 1997; Gonzalez et al., 2000). Although deletions that extend only a few residues into $S3_C$ do result in functional channels, they display more substantial gating perturbations (Gonzalez et al., 2000). Thus, this region of S3 may serve an important role as a component of the aqueous vestibule or crevice surrounding the S4 helix.

TABLE II

Residues Located at Kinks in Transmembrane α-Helices

Membrane protein	Transmembrane helix	Residues at kink
Bacteriorhodopsin (1AP9)	A	L22, **G23**
	B	V49, **P50**
	G	K216, V217, **G218**
Cytochrome *c* oxidase (1OCC)	I (I)	A26**, G27**
	II (I)	**G76**
	II (I)	M69, V70
	V (I)	**S198,** L199
	VI (I)	L248, **P249**
	X (I)	L381, **S382**
	XI (I)	**P427**, Q428
	II (II)	I67, L68, **P69**
	II (II)	L78, **P79**
	I (VIc)	V39, A40, E41
	I (VIII)	F26, L27
	I (VIII)	L37
Calcium pump (1EUL)	M3	**S261**
	M4	K297, I298
	M6	**G801**, L802
	M10	**S974**, L975, **P976**
Halorhodopsin (1E12)	A	**S32,** L33
	C	**S115**
	E	T181, D182
	G	K242, Y243
	F	W207, L208, **G209**
Photosynthetic reaction center (1PRC)	A (L)	**G45**, V46
	C (L)	C122, V123, **P124**
	C (L)	V133, F134
	E (L)	T241, L242
	C (M)	**G159,** C160
	E (M)	F269, F270, **S271**
Rhodopsin (1F88)	I	**G51,** F52, **P53**
	II	**G89**, **G90**
	III	**G120**
	V	F212, I213
	VI	C264, W265
	VII	**S298,** A299, V300

The first column gives the membrane protein name with PDB accession code indicated in parentheses. The transmembrane helices that have kinks are shown in the second column where for heteromultimeric proteins (Cytochrome *c* oxidase and Photosynthetic reaction center) the letters in parentheses indicate the subunit to which the helix belongs. The third column indicates the position and identity of residues found at kinks, with one line for each kink. Pro, Gly, and Ser residues are shown in bold.

We thank David Hackos for providing the Fourier transformation software and critical reading of the manuscript, and J. Nagle and D. Kauffman from the NINDS DNA sequencing facility for DNA sequencing.

Submitted: 26 October 2000
Revised: 10 January 2001
Accepted: 11 January 2001

REFERENCES

Blaber, M., X.J. Zhang, and B.W. Matthews. 1993. Structural basis of amino acid alpha helix propensity. *Science.* 260:1637–1640.

Cha, A., and F. Bezanilla. 1997. Characterizing voltage-dependent conformational changes in the *Shaker* K^+ channel with fluorescence. *Neuron.* 19:1127–1140.

Cha, A., and F. Bezanilla. 1998. Structural implications of fluorescence quenching in the *Shaker* K^+ channel. *J. Gen. Physiol.* 112: 391–408.

Cha, A., N. Zerangue, M. Kavanaugh, and F. Bezanilla. 1998. Fluorescence techniques for studying cloned channels and transporters expressed in *Xenopus* oocytes. *Methods Enzymol.* 296:566–578.

Cha, A., G.E. Snyder, P.R. Selvin, and F. Bezanilla. 1999. Atomic scale movement of the voltage-sensing region in a potassium channel measured via spectroscopy. *Nature.* 402:809–813.

Chuang, R.S., H. Jaffe, L. Cribbs, E. Perez-Reyes, and K.J. Swartz. 1998. Inhibition of T-type voltage-gated calcium channels by a new scorpion toxin. *Nat. Neurosci.* 1:668–674.

Cornette, J.L., K.B. Cease, H. Margalit, J.L. Spouge, J.A. Berzofsky, and C. DeLisi. 1987. Hydrophobicity scales and computational techniques for detecting amphipathic structures in proteins. *J. Mol. Biol.* 195:659–685.

Doyle, D.A., J.M. Cabral, R.A. Pfuetzner, A. Kuo, J.M. Gulbis, S.L. Cohen, B.T. Chait, and R. MacKinnon. 1998. The structure of the potassium channel: molecular basis of K^+ conduction and selectivity. *Science.* 280:69–77.

Gandhi, C.S., E. Loots, and E.Y. Isacoff. 2000. Reconstructing voltage sensor-pore interaction from a fluorescence scan of a voltage-gated K^+ channel. *Neuron.* 27:585–595.

Gonzalez, C., E. Rosenman, F. Bezanilla, O. Alvarez, and R. Latorre. 2000. Modulation of the Shaker K(+) channel gating kinetics by the S3–S4 linker. *J. Gen. Physiol.* 115:193–208.

Gray, T.M., and B.W. Matthews. 1984. Intrahelical hydrogen bonding of serine, threonine and cysteine residues within alpha-helices and its relevance to membrane-bound proteins. *J. Mol. Biol.* 175:75–81.

Hong, K.H., and C. Miller. 2000. The lipid–protein interface of a *Shaker* K^+ channel. *J. Gen. Physiol.* 115:51–58.

Komiya, H., T.O. Yeates, D.C. Rees, J.P. Allen, and G. Feher. 1988. Structure of the reaction center from *Rhodobacter sphaeroides* R-26 and 2.4.1: symmetry relations and sequence comparisons between different species. *Proc. Natl. Acad. Sci. USA.* 85:9012–9016.

Kubo, Y., T.J. Baldwin, Y.N. Jan, and L.Y. Jan. 1993. Primary structure and functional expression of a mouse inward rectifier potassium channel. *Nature.* 362:127–133.

Kyte, J., and R.F. Doolittle. 1982. A simple method for displaying the hydropathic character of a protein. *J. Mol. Biol.* 157:105–132.

Larsson, H.P., O.S. Baker, D.S. Dhillon, and E.Y. Isacoff. 1996. Transmembrane movement of the *Shaker* K^+ channel S4. *Neuron.* 16:387–397.

Li-Smerin, Y., and K.J. Swartz. 1998. Gating modifier toxins reveal a conserved structural motif in voltage-gated Ca^{2+} and K^+ channels. *Proc. Natl. Acad. Sci. USA.* 95:8585–8589.

Li-Smerin, Y., and K.J. Swartz. 2000. Localization and molecular determinants of the Hanatoxin receptors on the voltage-sensing domain of a K^+ channel. *J. Gen. Physiol.* 115:673–684.

Li-Smerin, Y., D.H. Hackos, and K.J. Swartz. 2000. α-Helical structural elements within the voltage-sensing domains of a K^+ channel. *J. Gen. Physiol.* 115:33–49.

MacArthur, M.W., and J.M. Thornton. 1991. Influence of proline residues on protein conformation. *J. Mol. Biol.* 218:397–412.

MacKinnon, R., S.L. Cohen, A. Kuo, A. Lee, and B.T. Chait. 1998. Structural conservation in prokaryotic and eukaryotic potassium channels. *Science.* 280:106–109.

Mannuzzu, L.M., M.M. Moronne, and E.Y. Isacoff. 1996. Direct physical measure of conformational rearrangement underlying potassium channel gating. *Science.* 271:213–216.

Mathur, R., J. Zheng, Y. Yan, and F.J. Sigworth. 1997. Role of the S3–S4 linker in *Shaker* potassium channel activation. *J. Gen. Physiol.* 109:191–199.

Monks, S.A., D.J. Needleman, and C. Miller. 1999. Helical structure and packing orientation of the S2 segment in the *Shaker* K^+ channel. *J. Gen. Physiol.* 113:415–423.

Monne, M., M. Hermansson, and G. von Heijne. 1999. A turn propensity scale for transmembrane helices. *J. Mol. Biol.* 288:141–145.

O'Neil, K.T., and W.F. DeGrado. 1990. A thermodynamic scale for the helix-forming tendencies of the commonly occurring amino acids. *Science.* 250:646–651.

Rees, D.C., L. DeAntonio, and D. Eisenberg. 1989a. Hydrophobic organization of membrane proteins. *Science.* 245:510–513.

Rees, D.C., H. Komiya, T.O. Yeates, J.P. Allen, and G. Feher. 1989b. The bacterial photosynthetic reaction center as a model for membrane proteins. *Annu. Rev. Biochem.* 58:607–633.

Rogers, J.C., Y. Qu, T.N. Tanada, T. Scheuer, and W.A. Catterall. 1996. Molecular determinants of high affinity binding of alpha-scorpion toxin and sea anemone toxin in the S3-S4 extracellular loop in domain IV of the Na^+ channel alpha subunit. *J. Biol. Chem.* 271:15950–15962.

Schrempf, H., O. Schmidt, R. Kummerlen, S. Hinnah, D. Muller, M. Betzler, T. Steinkamp, and R. Wagner. 1995. A prokaryotic potassium ion channel with two predicted transmembrane segments from *Streptomyces lividans. EMBO (Eur. Mol. Biol. Organ.) J.* 14:5170–5178.

Sorensen, J.B., A. Cha, R. Latorre, E. Rosenman, and F. Bezanilla. 2000. Deletion of the S3–S4 linker in the *Shaker* potassium channel reveals two quenching groups near the outside of S4. *J. Gen. Physiol.* 115:209–222.

Swartz, K.J. 1999. Inhibition of voltage-gated K^+ channel gating currents by hanatoxin. *Biophys. J.* 76:A150. (Abstr.)

Swartz, K.J., and R. MacKinnon. 1995. An inhibitor of the Kv2.1 potassium channel isolated from the venom of a Chilean tarantula. *Neuron.* 15:941–949.

Swartz, K.J., and R. MacKinnon. 1997a. Hanatoxin modifies the gating of a voltage-dependent K^+ channel through multiple binding sites. *Neuron.* 18:665–673.

Swartz, K.J., and R. MacKinnon. 1997b. Mapping the receptor site for hanatoxin, a gating modifier of voltage-dependent K^+ channels. *Neuron.* 18:675–682.

Takahashi, H., J.I. Kim, H.J. Min, K. Sato, K.J. Swartz, and I. Shimada. 2000. Solution structure of hanatoxin1, a gating modifier of voltage-dependent K^+ channels: common surface features of gating modifier toxins. *J. Mol. Biol.* 297:771–780.

Winterfield, J.R., and K.J. Swartz. 2000. A hot spot for the interaction of gating modifier toxins with voltage-dependent ion channels. *J. Gen. Physiol.* 116:637–644.

Yang, N., A.L. George, Jr., and R. Horn. 1996. Molecular basis of charge movement in voltage-gated sodium channels. *Neuron.* 16: 113–122.

Yellen, G. 1998. The moving parts of voltage-gated ion channels. *Q. Rev. Biophys.* 31:239–295.